Structure and electronic properties of cerium orthophosphate: Theory and experiment

Nicole Adelstein, B. Simon Mun, Hannah L. Ray, Philip N. Ross, Jr., Jeffrey B. Neaton, and Lutgard C. De Jonghe

Phys. Rev. B **83**, 205104 — Published 6 May 2011

DOI: 10.1103/PhysRevB.83.205104

Structure and Electronic Properties of Cerium Orthophosphate: Theory and Experiment

Nicole Adelstein[1,3], B. Simon Mun[4], Hannah L. Ray[1,3], Phillip N. Ross Jr.[1], Jeffrey B. Neaton,[2] and Lutgard C. De Jonghe[1,3]

[1]Materials Sciences Division
[2]Molecular Foundry
Lawrence Berkeley National Laboratory, 1 Cyclotron Road, Berkeley CA 94720, USA

[3]Department of Materials Science and Engineering
University of California at Berkeley, Berkeley CA 94720, USA

[4]Department of Applied Physics
Hanyang University, ERICA, Gyeonggi 426-791 Republic of Korea

Abstract

Using a combination of density functional theory (DFT) calculations and experiments, we determine the structural and electronic properties of cerium orthophosphate ($CePO_4$), a promising proton-conducting electrolyte for fuel cell applications. To better account for strongly-localized Ce 4f electrons, we use the DFT+*U* approach, where the exchange-correlation functional is augmented with an adjustable effective Hubbard-like parameter *U*. We find that the calculated structural properties are in good agreement with x-ray diffraction measurements, largely independent of the value of *U* used. However, the electronic structure is much more sensitive to *U*, and values of *U* = 2.5-3 eV for Ce 4f states provide excellent agreement between the calculated density of states and measured photoemission spectra near the valence band edge, and validate the efficacy of a DFT+*U* -based approach for this system. With a judicious choice of *U* determined from photoemission experiments, this work provides a natural starting point for future studies of charge transport and charged defect formation and migration in this important class of compounds.

I. Introduction

New materials with high proton conductivities in the temperature range 300-500°C can be of benefit as solid electrolytes in a variety of electrochemical devices such as hydrogen sensors, hydrogen separation membranes, and fuel cells. Incorporation of such a material into a fuel cell would, for example, facilitate the *in-situ* reforming of liquid biofuels and reduce the need for noble catalysts. Rare-earth phosphates have been investigated for this purpose because of their stability at high temperatures, and their ability to incorporate protons when doped with aliovalent cations [1-4].

Recent AC impedance spectroscopy for $CePO_4$ [2] indicates a total conductivity in air an order of magnitude higher than that of $LaPO_4$, a well-known proton-conductor. The enhanced conductivity of $CePO_4$ relative to its La-based counterpart has been attributed to hole conduction, based on defect chemistry interpretations of the measured conductivity in both wet versus dry conditions and reducing versus oxidizing environments [2]. First-principles calculations using density functional theory (DFT) can potentially elucidate the differences between $CePO_4$ and $LaPO_4$ conductivities. However, whereas ground-state electronic structure and proton conduction have already been studied with DFT for $LaPO_4$ [5], the electronic structure of $CePO_4$ is entirely unexplored. In $CePO_4$, highly-localized f-electrons can result in strong correlations that affect electronic structure and defect formation.

In this work, we show that the ground-state geometry and electronic structure of $CePO_4$ can be obtained with good accuracy using DFT-based methods via direct comparison to X-ray diffraction measurements and photoemission spectroscopy. We address the impact of the strongly-localized Ce 4f states with an adjustable effective Hubbard-like parameter *U*, and use photoemission data to determine the *U* that best describes the electronic structure of Ce for this system. A direct comparison between photoemission spectra and DFT-based electronic structure has not been made for a phosphate material, and as $CePO_4$ is just one of many phosphates, such as $FePO_4$,[6] being investigated as an ionic conductors for technological applications, we expect our approach and these results will be of

broad interest for both f-electron and phosphate-based solid-state electrolyte materials.

Cerium cations in solid-state compounds can exist in both the 3^+ and 4^+ oxidation states. The nominal charge on cerium in $CePO_4$ is Ce^{3+}, leaving one 4f electron on each cerium atom. The highly localized nature of these 4f states demands special consideration for the electronic structure of $CePO_4$. For cerium oxides, many groups [7-10] have recently documented the failure of standard DFT within the local density or generalized gradient approximations (LDA and GGAs) due to significant self-interaction errors associated with 4f electron states. For example, erroneous structural parameters have been reported, as well as, in some cases, metallic behavior for Ce-based compounds known to be insulators [11]. A common framework used to address these deficiencies is the DFT + *U* method[12]. In this approach, the strong Coulomb repulsion between localized *4f* states in Ce is treated by adding an effective Hubbard term to the Kohn-Sham Hamiltonian, leading to an improved description of correlation effects in transition-metal oxides. DFT + *U* requires two parameters, the Hubbard parameter *U* and the exchange interaction *J*. Since there is no unique way of including a Hubbard term within the DFT framework[12], different approaches may be adopted. In what follows, we use the rotationally invariant method of Dudarev *et al*. [13], a standard approach which is summarized in Ref. 13 and elsewhere.

Appropriate values of *U* for Ce 4f electrons have been debated in the literature and several *ab initio* and empirical values have been reported. Many prior studies use a value of *U* around 6 eV based on Slater integral calculations of metallic Ce[14] and cerium compounds[15] or optical band gaps and defect formation energies of cerium compounds[9, 16, 17]. However, significantly smaller values of *U* have also been reported for cerium oxides based on *ab initio* calculations[8], and comparison to lattice constants and energies of formation[7, 18]. Fabris *et al*. [8], for example, used a linear response approach[19] for CeO_2 and Ce_2O_3 and found *U* = 3 eV (LDA) and 1.5 eV (GGA). All studies noted that both the electronic structure and lattice parameters were somewhat sensitive to the value of *U*, although in different ways for CeO_2 and

Ce_2O_3, indicating that the best choice for *U* may depend on the environment of the cerium atom. Thus, it is prudent to determine an appropriate value for *U* by comparison to experiment for cerium in a phosphate environment – where Ce would be expected to behave differently than in cerium oxides or pure metal – rather than adopting values found in the literature for other cerium compounds.

In the following sections, ground-state structure and electronic properties of $CePO_4$ are computed using DFT+*U* for several different values of *U* and compared with X-ray diffraction (XRD), X-ray photoemission spectrometry (XPS), and AC impedance spectroscopy experiments on sintered, polycrystalline samples. We propose an optimal value of *U* that results in calculated electronic structure in agreement with measured photoemission near the valence band edge. This approach to determining *U* has yet to be used in *ab initio* studies of cerium compounds. We show that our value of *U* provides structural parameters that agree well with XRD measurements, thus providing a necessary foundation for future calculations of electron and proton conductivity, defect energetics, and redox reactions associated with the electrolytic performance of $CePO_4$.

II. Experimental Methods

Cerium orthophosphate powders, purchased from Alfa Aesar, are heat treated for 1 hour at 800°C in order to convert from the hydrated rhabdophane to the monoclinic phase. Powders are ground and sieved through 325 mesh, and then ball milled in isopropyl alcohol with 2 wt% PolyvynalVB, DiButal Phthalate, Manhaden Fish Oil (from Aldrich, Mallinckrodt, and Sigma, respectively) for 24 hours. The powders are dried, ground, and sieved again, and then uniaxially die pressed at 2000 psi into pellets. Pellets are heated to 600°C for 1h to remove binders and then heated to 1200°C for 5 hours for sintering. X-ray diffraction scans of powders and pellets are performed on a Philips PW3040 X'Pert Pro diffractometer using the Cu Kα (λ = 1.5406 Å) source operated with a 45 keV X-ray tube voltage.

A Kratos AXIS-NOVA Hemispherical electron analyzer is used for the measurement of XPS. The monochromatic Al K_α (photon energy =1486.6eV) is used as the x-ray source, and the total energy resolution is set to ~0.4 eV. The pass energy and dwell time of photoemission spectra is set to 20 eV and 100 msec, respectively. Prior to the XPS measurement, the sample surface is lightly sputtered with argon to remove any surface contamination. Sputtering does not change the oxidation state, as was shown by Glorieux in the $CePO_4$ spectra of the 3d binding energies [20]. A small charging effect is present during the measurement, and a low-energy electron flood gun is utilized when necessary. All elements in the sample are identified from a survey scan and the chemical state of each element is also confirmed. In order to compare the DFT density of states to the photoemission spectra, the Shirley background is subtracted from measured valence band spectra to remove the effects of inelastic scattering [21].

III. Computational methods

To compute the structure and electronic properties of $CePO_4$, we use DFT+*U* with both the local spin-density approximation (LSDA or, for short in this work, LDA) and the spin-dependent generalized gradient approximation (GGA) [22]. All results are obtained using the projector augmented-wave (PAW) method [23] as implemented in the Vienna *ab initio* Simulation Package (VASP) [24-26]. For comparison with XPS, spin-orbit coupling and the PBE0 hybrid functional is also employed [27]. We treat explicitly 12 electrons for cerium ($5s^25p^66s^25d^14f^1$), 5 for phosphorus ($2s^22p^5$), and 6 for oxygen ($2s^22p^6$). Brillouin zone integrations are performed with a Gaussian broadening of 0.1 eV during all calculations, a 6x6x6 Monkhorst-Pack k-point mesh with the original packing scheme [28], and a 600 eV plane-wave cutoff, all of which result in good convergence of the ground-state properties reported here. Energies are converged to 10^{-6} eV and Hellmann-Feynman forces on the ions are converged to 10 meV/Å. The equilibrium cell volume and shape are determined by optimizing all internal degrees of freedom with different functionals and values of *U*. The bulk modulus is calculated two ways, first by relaxing the ion position only and second by relaxing the cell shape and ion

positions. Both values are found to be consistent, and the latter is reported. The range of volumes used for the bulk modulus calculations is within 4-5% of the minimum volume.

As described above, it is well known that standard approximations to DFT, with or without gradient corrections, may incorrectly capture the electronic structure of materials with localized d or f states. In this work, we use a standard DFT+*U* framework, described in detail by Dudarev *et al.* [13], to correct for self-interaction errors associated with the Ce 4f states. In this approach, only an effective Hubbard parameter $U_{eff} = U - J$ enters the Hamiltonian. Here, we vary U_{eff} (which we simply refer to as *U* from here on) from 0 to 5 eV. (The standard DFT result corresponds to *U*=0 eV.)

IV. Results and Discussion

A. Structural properties

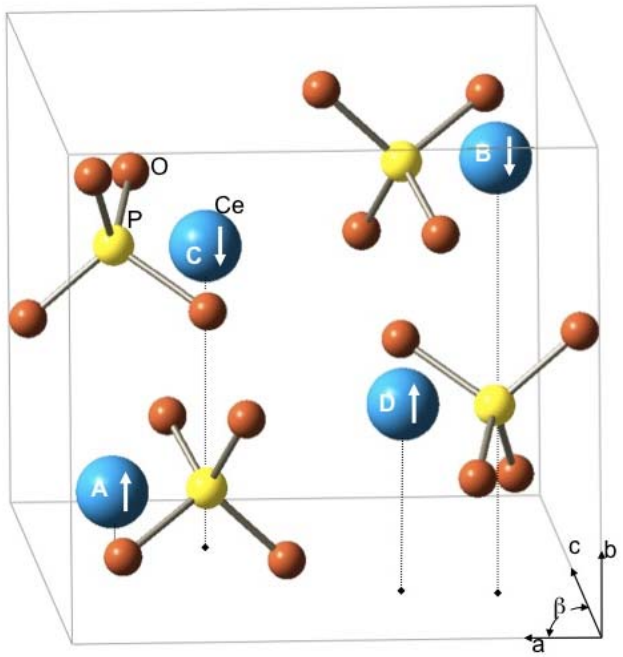

Figure 1: The conventional $CePO_4$ unit cell. The lattice vectors are **a**, **b**, and **c**, while the angle between **a** and **c** is β. The cerium cations are shown in blue, the tetrahedra are made of orange oxygen atoms and yellow

phosphorus atoms. An antiferromagnetic spin ordering of the cerium atoms is indicated with up and down arrows.

The monoclinic phase of $CePO_4$ assumes a structure with $P2_1/n$ symmetry (Fig 1) [29]. All atoms sit on sites that have the same symmetry and assume the 4e Wyckoff position, with coordinates: 'A' (x,y,z), 'B' (-x,-y,-z), 'C' (-x+1/2,y+1/2,-z+1/2), and 'D' (x+1/2,-y+1/2,z+1/2). There is a single unique cerium site, one phosphorous site, and four oxygen sites. $CePO_4$ is known to be antiferromagnetic (AFM) below a Neel temperature of 77 K[30]. Since there are four cerium atoms in the unit cell, for AFM ordering two must be spin-up and two must be spin-down (Fig 1). For U=0, our calculations of different spin configurations indicate the ground-state is ferromagnetic; for U ≥ 1 eV, however, our calculations predict the lowest energy spin arrangement is indeed AFM, in agreement with experiment. A small but non-negligible amount of hybridization between cerium 4f and oxygen 2p suggests that the AFM ordering found for finite values of U is mediated by superexchange. In the AFM ground state, each cerium atom has six Ce nearest-neighbors; two neighbors are spin-aligned and four are anti-aligned. For the remainder of the work, we assume the spin arrangement shown in Figure 1 for all calculations.

As expected, we find that the DFT+U approach within LDA generally results in smaller lattice parameters than the experiment for all values of U explored, leading to a 7% reduction in volume relative to room temperature measurements. In contrast, GGA-PBE predicts lattice parameters larger than experiments for all values of U, leading to an overestimation of the volume by at most 4%, as shown in Table 1a. In general, a larger U results in a larger predicted volume, although the change in volume for reasonable U is far less than typical errors associated with the LDA and GGA. In all cases, computed Wyckoff positions are in very good agreement with experiment and independent of U, as can be seen Table 1b.

Table 1a: The volume and lattice parameters for the measured and calculated $CePO_4$ unit cell are shown for selected *U*. The experimental bulk modulus (B) has not been reported.

Functional	Volume (Å^3)	a (Å)	b (Å)	c (Å)	β (deg)	B (GPa)
Experiment	300.60	6.8004	7.0231	6.4717	103.460	NA
LDA U=0	287.37	6.6935	6.9266	6.3705	103.357	125
U=3	290.20	6.7141	6.9515	6.3934	103.464	129
U=5	291.51	6.7204	6.9616	6.4040	103.351	133
PBE U=0	308.42	6.8956	7.0893	6.4980	103.849	99
U=3	310.84	6.9091	7.1084	6.5195	103.883	103
U=5	312.38	6.9156	7.1235	6.5304	103.832	103

1b: Atom positions (in reduced units of the lattice parameters) for selected values of *U* (in eV).

	Experiment	LDA U=0 eV	LDA U=3 eV	PBE U=0 eV	PBE U=3 eV
Ce x	0.2818	0.2800	0.2813	0.2852	0.2860
y	0.1591	0.1587	0.1586	0.1583	0.1586
z	0.1000	0.1032	0.1023	0.0992	0.0991
P x	0.3050	0.3039	0.3047	0.3039	0.3046
y	0.1663	0.1642	0.1641	0.1621	0.1621
z	0.6124	0.6144	0.6136	0.6116	0.6111
O1 x	0.2494	0.2486	0.2494	0.2498	0.2505
y	0.0059	0.0041	0.0047	0.0057	0.0061
z	0.4439	0.4438	0.4433	0.4405	0.4405
O2 x	0.3813	0.3817	0.3827	0.3813	0.3822
y	0.3314	0.3343	0.3333	0.3311	0.3303
z	0.4995	0.4964	0.4959	0.4987	0.4984
O3 x	0.1061	0.4771	0.4770	0.4714	0.4714
y	0.2163	0.1067	0.1084	0.1034	0.1035
z	0.8040	0.8096	0.8089	0.8067	0.8061
O4 x	0.1282	0.1243	0.1256	0.1273	0.1282
y	0.2163	0.2158	0.2158	0.2124	0.2125
z	0.7086	0.7152	0.7136	0.7099	0.7086

For LDA, the monoclinic angle β (Fig. 1) is computed to be between 103.3° and 103.6° for LDA depending on *U*, which brackets the experimental value of 103.47°. For GGA-PBE, the range of computed β values is between 103.8° and 104.0°. The experimental bulk modulus has not been reported, but the calculated values for GGA-PBE range between 99 and 103 GPa and the LDA values range between 123 and 133 GPa (Table 1a).

In summary, there is minimal variation in the structural parameters with *U,* aside from a slight increase in volume and bulk modulus with increasing *U*. Since a detailed comparison of calculated structural parameters to experiment does not point to a single 'best' value of *U*, in what follows we suggest an optimal *U* for Ce in $CePO_4$ through comparison to measured photoemission spectra.

B. Electronic Properties

In Fig. 2, we plot the density of states for $CePO_4$ for two different values of *U*. In contrast to the lattice parameters, the computed electronic structure depends significantly on the value of *U*, as expected. Notably, despite the fact that $CePO_4$ is known to be antiferromagnetic insulator, $CePO_4$ is computed as metallic and ferromagnetic for *U*=0, with the Fermi level positioned within the 4f states. However, for U ≥ 1 eV, the partial self-interaction correction associated with *U* reduces the occupied levels relative to the unoccupied states in the 4f manifold, opening an energy gap, and $CePO_4$ is correctly predicted to be insulating and antiferromagnetic. The band gap is found to grow with increasing *U*, as indicated in Fig. 2. There is sharp peak at the valence band edge associated with a lone Ce 4f electron per atom, reflecting a 3+ oxidation state for the Ce cation (confirmed via examination of the partial density of states).

Fig. 2 also shows that the gap between this occupied Ce 4f band and the top of the oxygen 2p band -- which will be referred to as the "valence gap" -- *decreases* with increasing *U* (peaks labeled in Fig 2 and Fig 3). Although *U* reduces the spurious self-interaction for 4f electrons, lowering the average energy of the occupied 4f bands, it does not affect the energetics of the O 2p band. In what follows, the valence gap is calculated as a function of *U* as the difference between energy levels at the M point, which represents the location of the direct "valence" gap between bands, as shown in Fig 3, where the full band structure is plotted.

Fig. 3 lends insight into the difference in conductivity between the lanthanum and cerium orthophosphates. p-type doping would lead to a partially-occupied 4f band at the Fermi level valence band, and extraordinarily heavy holes

(~1000m_e, where m_e is the electron mass) within an effective mass picture, due to the flatness of the bands. Interestingly, this would support hypotheses put forth in the literature that in oxidizing conditions conductivity is due to electron-hole hopping rather than proton transport based on the lack of H/D isotope effect[2] and the activated behavior of electronic conductivity seen in $CePO_4$.

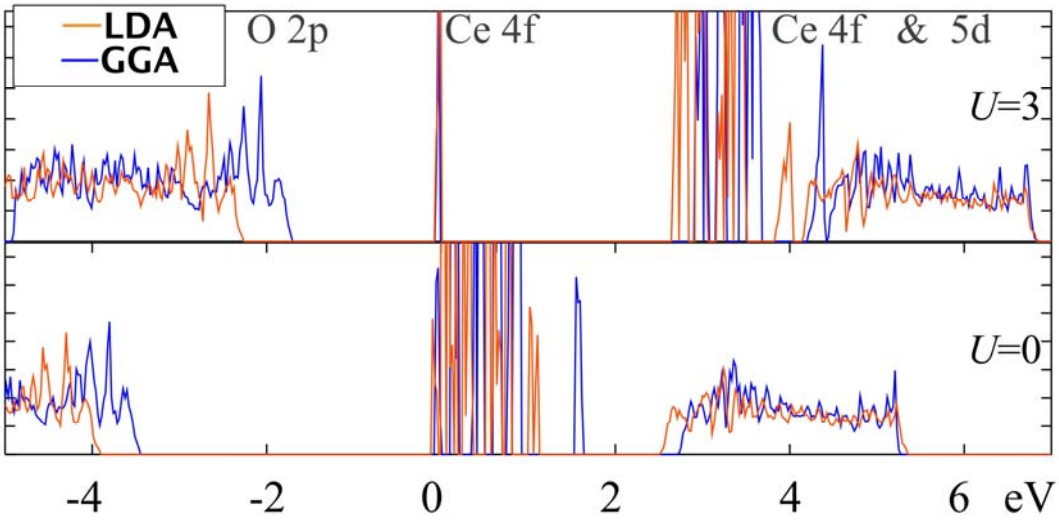

Figure 2: The valence and conduction bands for U=0 and 3; the other values of U follow this trend. The orange is the LDA functional and the blue is the GGA functional. The Fermi Energy is set to 0 eV and the orbital assignments at the top of the plot are from the partial DOS (which is not shown).

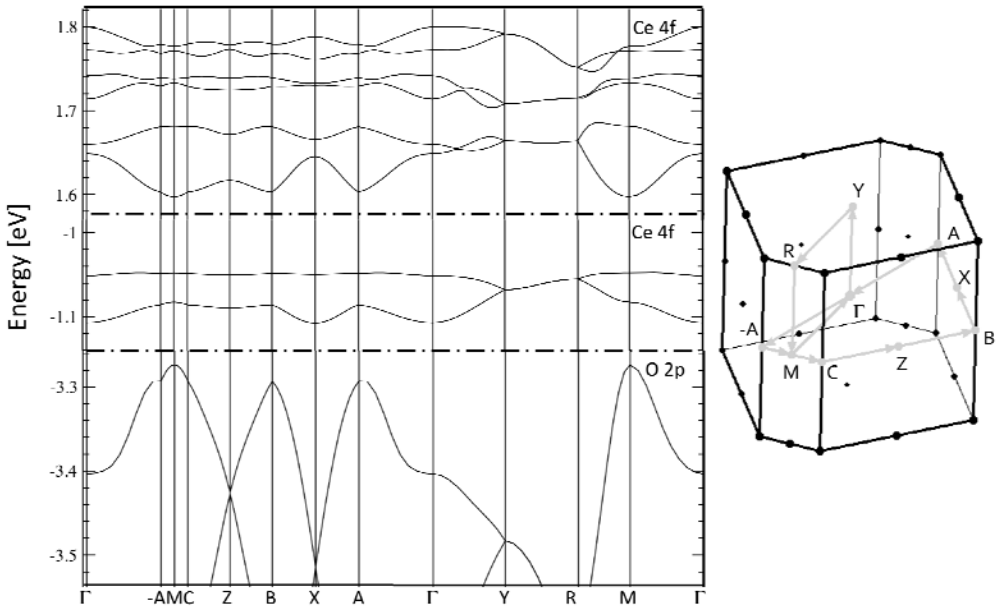

Figure 3: The band structure for LDA U=3 eV was calculated along lines between high symmetry points in the first Brillouin Zone, which are given in the plot to the left. High symmetry points are provided reduced coordinates of the primative reciprocal lattice vectors are: Γ (0,0,0), A(−0.60,0,0.41), B(0.40,0,0.41), C(−0.40,0,0.59), M(−0.5,0,0.5), R (−0.5,0.5,0.5), X (0.5,0,0.5), Y(0,0.5,0), and Z (0,0,0.5).

In Fig. 4a, we show the measured photoemission data taken on high purity cerium orthophosphate powders. From Fig. 4a, the measured valence energy gap is 2.5 ± 0.2 eV. As photoemission measures ejected electrons, it provides a good measure of the occupied density of states. The quasiparticle spectrum measured by photoemission can differ significantly from the Kohn-Sham density of states. Self-energy corrections to the Kohn-Sham energies, within the GW approximation for example, can account for these differences and lead to quantitative agreement with experiments[31,32]. In what follows, we adjust U, which can be viewed as a model self-energy correction to the 4f states, until the valence band agrees with the photoemission measurement.

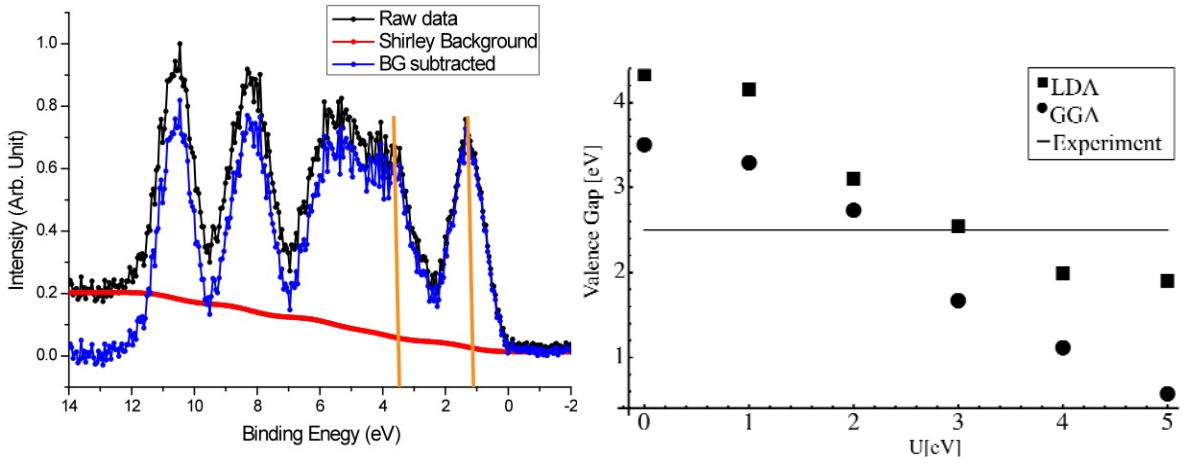

Figure 4a: The energy difference between the first two valence bands, measured peak to peak, is 2.5 +/- 0.2 eV. 4b: The energy difference between these two bands as measured by DFT+*U* for *U*=0-5 eV is plotted for LDA and GGA.

In Fig. 4b we plot the computed valence gap as a function of *U* for both LDA and GGA. As *U* partially corrects for the self-interaction associated with the 4f states, it will reduce their average energy relative to the O 2p band, causing a decrease in the valence gap with increasing *U*. The values of *U* that result in a valence gap closest to experiment are *U* = 3 eV for LDA and *U*= 2.5 eV for GGA. (We note that in determining these values, we have used the fully-optimized geometry for each of the two exchange-correlation functionals at a given value of *U*.) Interestingly, the computed valence gap does not decrease linearly with increasing *U*; it contains an inflection point for both LDA and GGA, as shown in Fig 4b. This "crossover" separates values of U large enough so that unoccupied Ce 4f states begin to overlap with the Ce 5d bands. Fig. 4b indicates a leveling off of the valence gap after *U* = 4 eV for LDA, which implies that this value of *U* is large enough to account for a majority of the self-interaction of the 4f orbitals, and that larger values will not significantly change the electronic structure. This "leveling off" is not observed for GGA up to 5 eV, though this may not be surprising since the inflection point in Fig 4b occurs for a larger value of *U* for GGA than for LDA.

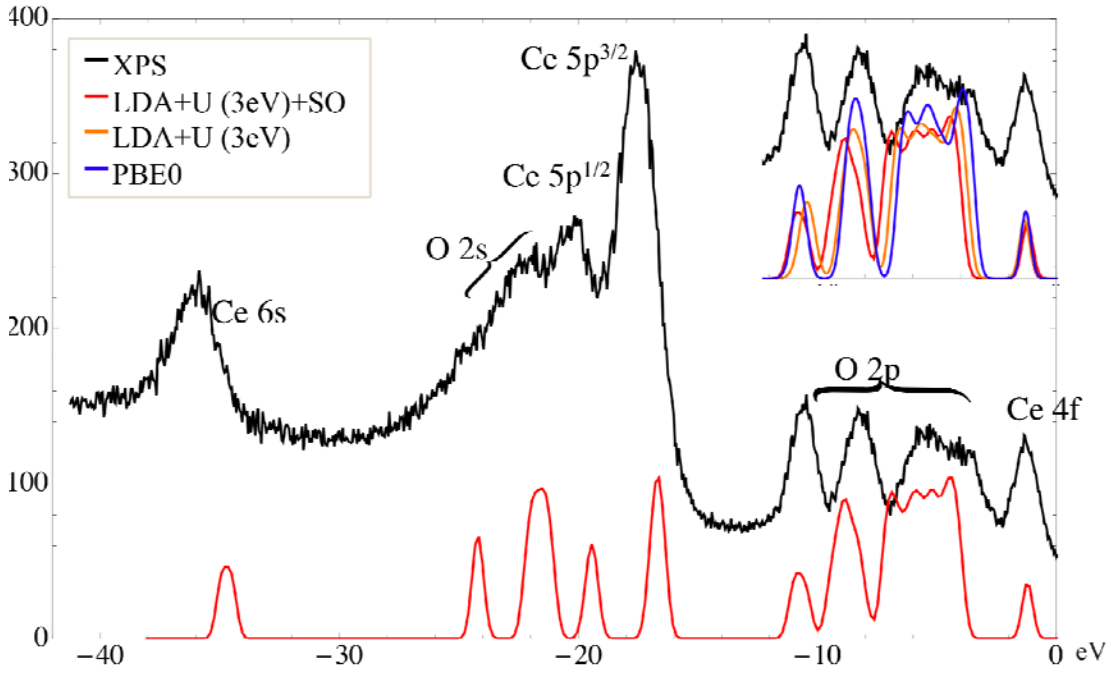

Figure 5: The valence band photoemission spectra is plotted along with the calculated density of states with Gaussian smearing for the LDA+*U* (3eV) plus spin-orbit (SO) coupling. The inset in the upper right compares the LDA+*U* and PBE0 near-valence band edge spectra. The peaks are assigned via the calculated partial density of states, and are supported by known XPS binding energies.

In Fig. 5, we present a direct comparison of the measured photoemission spectrum of $CePO_4$ and our first-principles calculations over a broad energy range. As described above, near the valence band edge the spectrum is best fit with *U*=3 eV for LDA. Peaks in the photoemission are assigned using a site- and orbital-projected DOS (not shown). Our assignments are very consistent with known literature values of the binding energies of these semi-core states (calibrated using the Ce *3d* peaks) [33]. To better capture the energetics of Ce states further below the valence band edge, spin-orbit corrections are also obtained with the VASP code, assuming noncollinear spins on the Ce ions [34, 35]. For *U* = 3 and within the LDA, we compute a 3 eV splitting of the Ce 5p orbitals, similar in magnitude to that predicted for CeF_3 [36]. (As expected, spin-orbit coupling has negligible influence on the electronic structure near the valence band edge.) We also compare our *U*=3eV LDA calculations with those using

a hybrid functional, PBE0[27, 37] which contains 25% Fock exchange. Use of hybrid functionals is an alternative to DFT+*U*, as they partially mitigate self-interaction errors for *all states*, not just the Ce 4f levels. We find small differences between the computed DOS for LDA *U* = 3eV and PBE0 for states further from the valence band edge, as expected; but from the inset of Fig. 5, the PBE0 valence gap is in good agreement with LDA *U* = 3eV, indicating that even when self-interaction corrections are also applied to O 2p states, fitting the Ce 4f *U* to the valence gap with a simpler DFT+*U* approach results in acceptable electronic structure for this compound.

Finally, we examine the question of why the LDA and GGA-PBE lead to different values of *U,* about 0.5 eV less for the GGA+*U* than LDA+*U* through comparison with photoemission experiments. We find that this distinction is primarily a consequence of the difference in the equilibrium volumes for the two functionals. We compute the DOS with LDA+*U* = 3 eV with the volume artificially fixed at the GGA+*U*=3eV volume (310.84 Å^3) and compare the result directly with LDA+*U*=3eV DOS at its true optimized volume (290.20 Å^3). A similar "computational experiment" is performed using GGA+*U*=3eV at both LDA+*U* and GGA+*U* volumes (290.20 Å^3 and 310.84 Å^3, respectively). For fixed volume and *U*, LDA+*U* and GGA+*U* yield very similar valence gaps (between Ce 4f and O 2p). Interestingly however, the band gap (between occupied and unoccupied 4f states) does depend somewhat more on the type of exchange-correlation functional. In sum, these "computational experiments" show that while specifics of the functional play a small role in the electronic structure, the valance gap (and value of *U* that best fits it) is most sensitive to cell volume. We note here that since the LDA and GGA used here bracket the experimental volume, our work demonstrates that for $CePO_4$, *U* lies in the range of 2.5-3 eV.

IV. Conclusions

The ground-state geometry and electronic structure of $CePO_4$ was investigated with X-ray diffraction and photoemission, and a DFT+*U* method for Hubbard-like effective *U* values ranging from 0-5 eV. We found that structural properties, including lattice parameters and bulk moduli, are not sensitive to *U*. In contrast however, the electronic structure is strongly sensitive to U near the band edges, as expected. By direct comparison with experiments, we found that the *U* values for Ce 4f states in $CePO_4$ that provide the best match for experiments were between 2.5 and 3 eV. More specifically, we computed that *U*=3 eV for LDA functional and *U*=2.5 eV for the GGA-PBE functional by comparing directly to the "valence gap", defined here as the difference between the bottom of the occupied 4f and the top of the occupied O 2p valence bands. The smaller value of *U* for GGA can be primarily associated with its larger unit cell volume. Using a density of states computed with LDA+*U*=3 eV, all peaks in the photoemission spectrum could be assigned with confidence. The use of the non-empircal PBE0 functional to calculate the density of states confirmed that even when self-interaction errors are treated for all states, fitting the valence gap is acceptable to fix the *U* for Ce 4f electrons. The calculations presented here show the importance of using photoemission spectroscopy for validating *U* parameters. This work sets the stage for further theoretical work on proton hopping in $CePO_4$ and the electronic structure of aliovalently doped and oxygen deficient $CePO_4$, and will inevitable lend insight into the nature of the mixed-conduction of this proton-conducting material.

Acknowledgments

This work was supported by the Director, Office of Science, Office of Basic Energy Sciences, Materials Sciences and Engineering Division, of the U.S. Department of Energy under Contract No. DE-AC02-05CH11231. Work at the Molecular Foundry was supported by the Office of Science, Office of Basic Energy Sciences, of the U.S. Department of Energy under Contract No. DE-AC02-05CH11231. We also gratefully acknowledge computational support from NERSC, which is supported by the Office

of Science of the U.S. Department of Energy under Contract No. DE-AC03-76SF00098.

1. T. Norby, Nature **410** (6831), 877-878 (2001).
2. N. Kitamura, K. Amezawa, Y. Tomii, T. Hanada, N. Yamamoto, T. Omata and S. Otsuka-Yao-Matsuo, J. Electrochem. Soc. **152** (4), A658-A663 (2005).
3. E. G. del Moral, D. P. Fagg, E. Chinarro, J. C. C. Abrantes, J. R. Jurado and G. C. Mather, Ceram. Int. **35** (4), 1481-1486 (2009).
4. G. Harley, K. D. Kreuer, J. Maier and L. C. De Jonghe, J. Non-Cryst. Solids **355** (16-17), 932-937 (2009).
5. R. Yu and L. C. De Jonghe, J Phys Chem C **111** (29), 11003-11007 (2007).
6. F. Zhou, K. S. Kang, T. Maxisch, G. Ceder and D. Morgan, Solid State Commun **132** (3-4), 181-186 (2004).
7. J. L. F. Da Silva, M. V. Ganduglia-Pirovano, J. Sauer, V. Bayer and G. Kresse, Phys Rev B **75** (4) (2007).
8. S. Fabris, S. de Gironcoli, S. Baroni, G. Vicario and G. Balducci, Phys Rev B **71** (4) (2005).
9. J. Kullgren, C. W. M. Castleton, C. Muller, D. M. Ramo and K. Hermansson, Journal of Chemical Physics **132** (5) (2010).
10. G. Pacchioni, J. Chem. Phys. **128** (18) (2008).
11. K. Terakura, T. Oguchi, A. R. Williams and J. Kubler, Phys Rev B **30** (8), 4734-4747 (1984).
12. V. I. Anisimov, F. Aryasetiawan and A. I. Lichtenstein, J. Phys.-Condes. Matter **9** (4), 767-808 (1997).
13. S. L. Dudarev, G. A. Botton, S. Y. Savrasov, Z. Szotek, W. M. Temmerman and A. P. Sutton, Phys. Status Solidi A-Appl. Res. **166** (1), 429-443 (1998).
14. A. I. Lichtenstein and M. I. Katsnelson, Phys Rev B **57** (12), 6884-6895 (1998).
15. A. I. Liechtenstein, V. P. Antropov and B. N. Harmon, Phys Rev B **49** (15), 10770-10773 (1994).
16. C. Sevik and T. Cagin, Phys Rev B **80** (1) (2009).
17. Y. Jiang, J. B. Adams and M. van Schilfgaarde, Journal of Chemical Physics **123** (6) (2005).
18. J. L. F. Da Silva, M. V. Ganduglia-Pirovano and J. Sauer, Phys Rev B **76** (12) (2007).
19. M. Cococcioni and S. de Gironcoli, Phys. Rev. B **71** (3) (2005).
20. B. Glorieux, R. Berjoan, M. Matecki, A. Kammouni and D. Perarnau, Appl. Surf. Sci. **253** (6), 3349-3359 (2007).
21. M. Repoux, Surf. Interface Anal. **18** (7), 567-570 (1992).
22. J. P. Perdew, K. Burke and M. Ernzerhof, Phys. Rev. Lett. **77** (18), 3865-3868 (1996).
23. P. E. Blochl, Phys Rev B **50** (24), 17953-17979 (1994).
24. G. Kresse and J. Furthmuller, Comput. Mater. Sci. **6** (1), 15-50 (1996).
25. G. Kresse and J. Furthmuller, Phys. Rev. B **54** (16), 11169-11186 (1996).
26. G. Kresse and J. Hafner, Phys Rev B **47**, 558 (1993).

27. C. Adamo and V. Barone, J. Chem. Phys. **110** (13), 6158-6170 (1999).
28. H. J. Monkhorst and J. D. Pack, Phys. Rev. B **13** (12), 5188-5192 (1976).
29. G. W. Beall, L. A. Boatner, D. F. Mullica and W. O. Milligan, Journal of Inorganic & Nuclear Chemistry **43** (1), 101-105 (1981).
30. F. D. Srygley and L. K. Wilson, Bulletin of the American Chemical Society **24** (2) (1979).
31. M. S. Hybertsen and S. G. Louie, Phys Rev B **34** (4), 2920-2922 (1986).
32. M. Shishkin, M. Marsman and G. Kresse, Phys. Rev. Lett. **99** (24) (2007).
33. A. Fujimori, Phys Rev B **28** (8), 4489-4499 (1983).
34. D. Hobbs, G. Kresse and J. Hafner, Phys Rev B **62** (17), 11556-11570 (2000).
35. M. Marsman and J. Hafner, Phys Rev B **66** (22) (2002).
36. K. Klier, P. Novak, A. C. Miller, J. A. Spirko and M. K. Hatalis, Journal of Physics and Chemistry of Solids **70** (9), 1302-1311 (2009).
37. J. Paier, M. Marsman and G. Kresse, J. Chem. Phys. **127** (2) (2007).